Salawu, S. O.; Kareem, R. A.; Shonola, S. A.

Article

Radiative thermal criticality and entropy generation of hydromagnetic reactive Powell-Eyring fluid in saturated porous media with variable conductivity

Energy Reports

Provided in Cooperation with:
Elsevier

Suggested Citation: Salawu, S. O.; Kareem, R. A.; Shonola, S. A. (2019) : Radiative thermal criticality and entropy generation of hydromagnetic reactive Powell-Eyring fluid in saturated porous media with variable conductivity, Energy Reports, ISSN 2352-4847, Elsevier, Amsterdam, Vol. 5, pp. 480-488, https://doi.org/10.1016/j.egyr.2019.04.014

This Version is available at:
https://hdl.handle.net/10419/243603

Energy Reports 5 (2019) 480–488

Contents lists available at ScienceDirect

Energy Reports

journal homepage: www.elsevier.com/locate/egyr

Research paper

Radiative thermal criticality and entropy generation of hydromagnetic reactive Powell–Eyring fluid in saturated porous media with variable conductivity

S.O. Salawu [a,*], R.A. Kareem [b], S.A. Shonola [c]

[a] Department of Mathematics, Landmark University, Omu-aran, Nigeria
[b] Department of Mathematics, Lagos State Polytechnic, Ikorodu, Nigeria
[c] Department of Mathematics, Coventry University, UK

ARTICLE INFO

Article history:
Received 1 April 2019
Received in revised form 22 April 2019
Accepted 25 April 2019
Available online xxxx

Keywords:
Inherent irreversibility
Non-Newtonian
Thermal runaway
Reactive fluid
Thermal radiation

ABSTRACT

Theoretical study of inherent irreversibility and thermal runaway of an exothermic reactive Eyring–Powell fluid flow through a saturated porous fixed horizontal channel with thermal radiation and variable electrical conductivity is investigated. The reactive conducting fluid under bimolecular chemical rate law is propelled by pressure gradient. Ignoring the material assumptions, the governing dimensionless equations of the flow model are solved using semi discretization finite difference techniques coupled with weighted residual method. The results in terms of flow rate, temperature, thermal runaway, Bejan number and entropy generation are presented in graphical form. From the results, it is observed that parameter which argument the entropy production rate also enhances the Bejan number. Also, minimization of entropy generation is achieved at low values of thermal radiation, dissipation rate, electric field loading and viscosity variables.

1. Introduction

The flow of electrically conducting fluid through a nonlinear saturated porous medium, and it interaction with magnetic fields has numerous applications in engineering and industrial phenomenons such as power nuclear reactor, soil science, crude oil purification, solar structures, MHD generator design an so on, Salawu and Dada (2016). Flow of hydromagnetic Newtonian fluid accompany with heat transfer under different geometries with various physical effects has been studied by many scientist due to it use in several devices and processes, (Adesanya et al., 2015; Rundora and Makinde, 2018). Recently, most studies focus on non-Newtonian fluid because of their usefulness and rheology features. Fluids such as polyphenyether, hydrocarbon oil, slurries, drilling mud etc portrayed properties that cannot be captured by Navier–Stokes formulation. Among the mechanics of fluid formulations that described the non-Newtonian characteristics is the third grade, casson, viscoelastic, Walters-B and Powell–Eyring fluids, found in (Okoya (2011); Ogunseye and Okoya (2017); Salawu et al. (2018); Cortell (2006); Gireesha et al. (2015); Mahanthesh et al. (2017)).

Of all the non-Newtonian fluid, Powell–Eyring fluid has special rheology properties that make it advantageous over other non-Newtonian fluids. Apart from the fact that it was gotten from the liquid kinetic theory, unlike fluids of power-law model which was obtained from empirical relation. Powell–Eyring fluid at large and small shear rate, it behaves like a Newtonian fluid. In view of these, Longo et al. (2013a,b, 2015) carried out experimental investigation of non-Newtonian power-law flow in an axisymmetric permeable medium with currents gravity. Jalil et al. (2013) reported on similarity solutions for Powell–Eyring fluid flow past a motioning plate. The authors transformed the main equations to an ordinary coupled differential equations using scaling group and then solved computationally by Keller-box techniques. Hayat et al. (2016) examined Eyring–Powell fluid under the effects of dufour, soret, joule heating and thermal radiation. The analysis was done using series solution and compared with numerical results. Rehman et al. (2016, 2017) investigated Powell–Eyring fluid with heat sink/source and mixed convection in an elongated cylinder. In the study, dual analysis of stratified parabolic and logarithmic curve fitting was done. Also, Akbar et al. (2015) discussed the computational solution of hydromagnetic Eyring–Powell boundary layer fluid flow past a stretching plate. (Di Federicoa et al. (2014); Longo et al. (2013a,b)) examined the theoretical and experimental solution of non-Newtonian power-law flow in porous media. Studies on Powell–Eyring fluid were done by authors without examined the rate of entropy generation due to irreversibility and thermal runaway as a result of temperature criticality.

* Corresponding author.
E-mail address: salawu.sulyman@lmu.edu.ng (S.O. Salawu).

https://doi.org/10.1016/j.egyr.2019.04.014

Analysis of the second law of thermodynamic studies entropy generation and reactive solution blowup are important in the heat transport mechanism. Many researcher have considered entropy generation in a system due to its effect on the efficiency of the thermal system designs. Minimization of entropy production in a MHD viscoelastic fluid flow in porous media was studied by Baag et al. (2017). The flow model was solved using Kummer's function and it was reported that at high values of viscoelastic and magnetic field variables, the velocity distribution decayed. Govindaraju et al. (2015) investigated entropy generation rate in a stretching surface of a magneto-hydrodynamic nanomaterial fluid. The authors applied Lie group transformation to the formulated equations to reduce the model to ODEs. Bhatti and Rashidi (2017) examined hydromagnetic stagnation nanofluid past an elongated surface with reduction of entropy generation in the system. The authors adopted linearization scheme coupled with spectral Chebyshev collocation techniques to solve the dimensionless equations. Hayat et al. (2017) studied entropy generation in a peristaltic flow under various shapes of nanoparticles. Celli et al. (2017) reported on the thermal stability of a two dimensional power-law liquid flow through a permeable open boundary layer. In the study, the experimental feasibility results was compared with the theoretical results for the stability analysis. Ogunseye and Okoya (2017) investigated in a cooling surface of cylindrical pipe, the thermal explosion and criticality of third grade fluid. Salawu and Okedoye (2018) examined second thermodynamic law of exothermic two-step reactive hydromagnetic fluid flow with heat absorption and convective cooling. In the study, the rate of entropy production in the system was investigated and reported. Some relevant articles on entropy generation in a thermal system are reported in (Khan et al. (2018); Hayat et al. (2018), Ahmed et al. (2018)). All the analysis on entropy generation was done without references to Powell–Eyring fluid and thermal runaway.

Studies associated to entropy generation, thermal runaway and heat transports in saturated porous media are essential in enhancing the design and operation of several devices in engineering. For example, the automobile's exhaust catalytic converter that offers a platform for exothermic reaction with complete hydrocarbons combustion. This process assist in reducing the toxic emissions such as carbon(II)oxide (CO) that pollute the environment. The aim of this study is to examine the thermal runaway and irreversibility process of a reactive Powell–Eyring fluid with variable electrical conductivity and thin thermal radiation via second thermodynamic law. The flow model is offered in Section 2, in Section 3, the numerical solution scheme is implemented. Section 4 covers the analysis of entropy generation while in Section 5, the results are presented in diagram form and discussed in respect to the effect of some parameters.

2. Mathematical formulation

Transient laminar isotropic flow of reactive combustible Eyring–Powell conducting fluid between fixed parallel walls of width h with a saturated porous medium is considered. The heat dependent pre-exponential factor variable and reactant diffusion is taken into account with the electric field E_y stimulating the magnetic field strength B_0. The channel walls temperature is non-uniform as illustrated in Fig. 1. The exothermic reaction is induced by the Bimolecular chemical kinetic law with $m = 0.5$ and at $\bar{t} \leq 0$, the heat combustive hydromagnetic fluid is assumed static while fully developed uniform pressure gradient encourages the flow at $\bar{t} > 0$. The non-Newtonian effect is by the Eyring–Powell Cauchy model defined as follows.

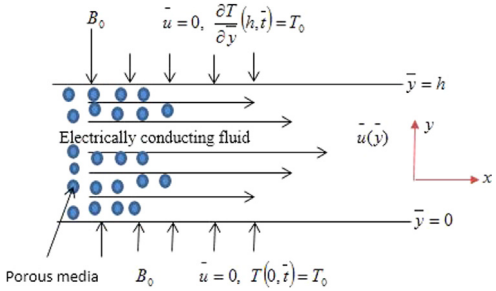

Fig. 1. The Geometry of the flow.

The Cauchy Eyring–Powell stress tensor fluid model is defined according to Hayat et al. (2013) as

$$V_{ij} = \frac{1}{\beta} sinh^{-1}\left(\frac{1}{\Lambda}\frac{\partial \bar{u}_i}{\partial \bar{y}_j}\right) + \mu\frac{\partial \bar{u}_i}{\partial \bar{y}_j}. \tag{1}$$

The term μ is the coefficient of fluid viscosity while Λ and β are the fluid material constant. That is,

$$sinh^{-1}\left(\frac{1}{\Lambda}\frac{\partial \bar{u}_i}{\partial \bar{y}_j}\right) \cong \frac{1}{\Lambda}\frac{\partial \bar{u}_i}{\partial \bar{y}_j} - \frac{1}{6}\left(\frac{1}{\Lambda}\frac{\partial \bar{u}_i}{\partial \bar{y}_j}\right)^3. \tag{2}$$

The heat dependent variable electrical conductivity $\sigma(T)$ for the reactive fluid under consideration is given as

$$\sigma(T) = \sigma_0\left(\frac{E(T - T_0)}{T_0^2 R}\right)^n. \tag{3}$$

where σ_0 is the wall electrical conductivity and n is the electrical conductivity exponent. Follow the assumptions above, the flow approximation boundary layer model equations for the momentum and temperature balance of the reactive Eyring–Powell fluid in a saturated porous medium are as follows:

$$\rho\frac{\partial \bar{u}}{\partial \bar{t}} = -\frac{\partial \bar{P}}{\partial \bar{x}} + \left(\mu + \frac{1}{\beta\Lambda}\right)\frac{\partial^2 \bar{u}}{\partial \bar{y}^2} - \frac{1}{2\beta\Lambda^3}\left(\frac{\partial \bar{u}}{\partial \bar{y}}\right)^2\frac{\partial^2 \bar{u}}{\partial \bar{y}^2} - \frac{\mu}{K}\bar{u} - \frac{b}{\sqrt{K}}\bar{u}^2 - \sigma(T)B_0(B_0\bar{u} + E_y). \tag{4}$$

$$\rho C_p\frac{\partial T}{\partial \bar{t}} = k\frac{\partial^2 T}{\partial \bar{y}^2} - \frac{\partial q}{\partial \bar{y}} + \sigma(T)(B_0\bar{u} + E_f)^2 + \frac{\mu}{K}\bar{u}^2 + \frac{b}{\sqrt{K}}\bar{u}^3 + QCA\left(\frac{KT}{vl}\right)^m e^{-\frac{E}{RT}} + \left(\frac{\partial \bar{u}}{\partial \bar{y}}\right)^2\left[\left(\mu + \frac{1}{\beta\Lambda}\right) - \frac{1}{6\beta\Lambda^3}\left(\frac{\partial \bar{u}}{\partial \bar{y}}\right)^2\right] \tag{5}$$

The boundary conditions for the flow model are as follows

$$\bar{u}(\bar{y}, 0) = 0,\ T(\bar{y}, 0) = T_a,\ \bar{u}(h, \bar{t}) = 0,\ \frac{\partial T}{\partial \bar{y}}(h, \bar{t}) = T_0,\ \bar{u}(0, \bar{t}) = 0,\ T(0, \bar{t}) = T_0 \ \text{ for } \bar{t} > 0. \tag{6}$$

where $\bar{P}$ is the pressure, $\bar{t}$ is time, $\bar{x}$ and $\bar{y}$ are respectively the distance measured in the axial and normal direction, T and $\bar{u}$ are respectively the reactive fluid temperature and velocity. c, K, m, ρ, k, A, E, C, R, Q, C_p, v and l are respectively the resistance constant porous inertia, permeability of the media, chemical kinetics, density, thermal conductivity, rate constant, activation energy, chemical species, gas universal constant, reaction heat, heat capacity, vibration frequency and planck's constant. As depicted in Eq. (6), the fluid velocity initial condition is zero. This shows that the fluid motion start from rest. The radiative flux differential

approximation q is defined by Makinde and Chinyoka (2010) as.

$$\frac{\partial}{\partial \bar{y}}\left(\frac{1}{a}\frac{\partial q}{\partial \bar{y}}\right) - 16a\sigma T^3\frac{\partial T}{\partial \bar{y}} - 3a^2 q = 0, \tag{7}$$

where σ denotes Stefan–Boltzmann constant and a denotes coefficient of absorption. Here, $a \ll 1$ is adopted for an optical thin case and the radiative flux approximation equation is taken as

$$\frac{\partial q}{\partial \bar{y}} = 4\sigma a(T_r^4 - T^4). \tag{8}$$

The quantities in Eqs. (8) and (9) are introduced into the Eqs. (4) to (6) above.

$$\begin{aligned}
&G = -\frac{\partial P}{\partial x}, y = \frac{\bar{y}}{h}, t = \frac{\mu \bar{t}}{h^2\rho}, x = \frac{\bar{x}}{h}, \phi = \frac{E_y}{B_0 U},\\
&u = \frac{\bar{u}}{U}, Ha = \frac{h^2\sigma_0 B_0^2}{\mu}, \theta = \frac{E(T-T_0)}{RT_0^2},\\
&\lambda = \frac{AChQ^2E}{k_0RT_0^2}\left(\frac{KT_0}{l\upsilon}\right)^n e^{-\frac{1}{\epsilon}}, Br = \frac{\mu EU^2}{Rk_0T_0^2}, \delta = \frac{U^2}{2\Lambda^2h^2},\\
&\alpha = \frac{1}{\mu\Lambda\beta}, \epsilon = \frac{RT_0}{E}, Pr = \frac{\mu c_p}{k_0},\\
&\theta_a = \frac{E(T_a - T_0)}{RT_0^2}, D = \frac{h^2}{K}, F = \frac{Uh^2b}{\mu\sqrt{K}}, P = \frac{\bar{P}h}{U\mu}, R = \frac{4a\sigma r^2T_r^3}{k}.
\end{aligned} \tag{9}$$

The main equations and the boundary conditions in dimensionless form become

$$\begin{aligned}
\frac{\partial u}{\partial t} &= \frac{\partial^2 u}{\partial y^2} - \delta\alpha\left(\frac{\partial u}{\partial y}\right)^2\frac{\partial^2 u}{\partial y^2} + (1+\alpha)\frac{\partial^2 u}{\partial y^2}\\
&\quad - Du - Fu^2 - Ha(u+\phi)\theta^n + G,
\end{aligned} \tag{10}$$

$$\begin{aligned}
Pr\frac{\partial \theta}{\partial t} &= \frac{\partial^2\theta}{\partial y^2} + Br\left[\left(\frac{\partial u}{\partial y}\right)^2\left((1+\alpha) + \frac{\alpha\delta}{3}\left(\frac{\partial u}{\partial y}\right)^2\right)\right.\\
&\quad \left. + Du^2 + Fu^3 + Ha(u+\phi)^2\theta^n\right] +\\
&R[(\theta+1)^4 - 1] + \lambda(1+\epsilon\theta)^m e^{\frac{\theta}{1+\epsilon\theta}}
\end{aligned} \tag{11}$$

The dimensionless boundary conditions

$$\begin{aligned}
&u(y,0) = 0,\ \theta(y,0) = \theta_a,\ u(1,t) = 0,\ \frac{\partial\theta}{\partial y}(1,t) = 0,\\
&u(0,t) = 0,\ \theta(0,t) = 0 \ \text{ for } t > 0.
\end{aligned} \tag{12}$$

where the parameter θ_a, u, θ, Ha, G, D, F, Pr, ϕ, Br, ϵ, λ and R are respectively the initial temperature, fluid velocity, fluid temperature, Hartmann number, pressure gradient, porous media, porous media of second order, Prandtl number, electric field loading, Brinkman number, activation energy, Frank-Kamenetskii, thermal radiation. The parameters δ and α are the Eyring–Powell material.

3. Numerical analysis

The computational algorithm employed is based on finite difference of semi-implicit method (Chinyoka and Makinde, 2013; Ireka and Chinyoka, 2013). Implicit terms are intermediary considered at the level of time $(p+\psi)$, for range [0,1]. Here, $\psi = 1$ is utilized to allow large time steps. The computational scheme used in this analysis is speculated to be effective for any time step value! The governing dimensionless equations is discretized based on Cartesian linear uniform grid and mesh. The central second order difference is used to approximate the spatial derivatives for the first and second order. The boundary conditions are integrated by modifying the contained last and first equations grid points. The numerical scheme is tested for stability and consistence. The velocity module for the semi-implicit scheme is presented as:

$$\begin{aligned}
&\frac{u^{(p+1)} - u^{(p)}}{\Delta t} = (1+\alpha)\frac{\partial^2}{\partial y^2}u^{(p+\psi)}\\
&+ G - \alpha\delta\left(\frac{\partial u}{\partial y}\right)^{2(p)}\frac{\partial^2}{\partial y^2}u^{(p+\psi)} - Du^{(p+\psi)} - Fu^{2(p+\psi)} -\\
&Ha\left(\phi + u^{(p+\psi)}\right)\left(\theta^n\right)^{(p)}.
\end{aligned} \tag{13}$$

The equation defining $u^{(p+1)}$ is written as:

$$\begin{aligned}
&-r_1u_{j-1}^{(p+1)} + \left(\Delta tHa\left(\theta^n\right)^{(p)} + 2r_1\right)u_j^{(p+1)} - r_1w_{j+1}^{(p+1)}\\
&= u^{(p)} + \Delta tG + \Delta t(1-\psi)(1+\alpha)u_{yy}^{(p)} -\\
&\Delta t(1-\psi)(Du^{(p)} + Fu^{2(p)}) - \Delta t(1-\psi)\alpha\delta\left(u_y\right)^{2(p)}u_{yy}^{(p)}\\
&- \Delta tHa(1-\psi)\left(\phi + u^{(p)}\right)\left(\theta^n\right)^{(p)}
\end{aligned} \tag{14}$$

where $r_1 = \psi\frac{\Delta t}{\Delta y^2}$. Thus, solution for $u^{(p+1)}$ leads to tri-diagonal inverse matrices. The integration semi-implicit scheme for temperature balance equation component takes after the velocity module scheme. The second unmixed derivatives for the heat balance are implicitly treated as follows:

$$\begin{aligned}
Pr\frac{\theta^{(p+1)} - \theta^{(p)}}{\Delta t} &= Br\left[\left(\frac{\partial u}{\partial y}\right)^2\left((1+\alpha) + \frac{\alpha\delta}{3}\left(\frac{\partial u}{\partial y}\right)^2\right)\right.\\
&\quad \left. + Du^2 + Fu^3 + Ha(u+\phi)^2\theta^n\right]^{(p)} +\\
&\frac{\partial^2}{\partial y^2}\theta^{(p+\psi)} + \lambda\left[(1+\epsilon\theta)^m e^{\frac{\theta}{1+\epsilon\theta}}\right]^{(p)} + R[(\theta^{(p)}+1)^4 - 1].
\end{aligned} \tag{15}$$

The equation defining $\theta^{(p+1)}$ becomes:

$$\begin{aligned}
&-r_1\theta_{j-1}^{(p+1)} + (Pr + 2r_1)\theta_j^{(p+1)} - r_1\theta_{j+1}^{(p+1)}\\
&= \lambda\left[(1+\epsilon\theta)^m e^{\frac{\theta}{1+\epsilon\theta}}\right]^{(p)} + R[(\theta^{(p)}+1)^4 - 1]\\
&Br\left[(u_y)^2\left((1+\alpha) + \frac{\alpha\delta}{3}(u_y)^2\right) + Du^2 + Fu^3 + Ha(\phi+u)^2\theta^n\right]^{(p)}\\
&+ \theta^{(p)} + \theta_{yy}^{(p)}.
\end{aligned} \tag{16}$$

The solution technique again change to tri-diagonal inverse matrices. The procedures (14) and (16) are second order in space and in time, it is accurate and consistence in first order at $\psi = 1$. Here, $\psi = 1$ is used for steady convergent solutions at high time steps. The algorithm was confirmed for temporal and spatial convergence. In fact, the solution at $\Delta t = 1$ with 150 steps time are equal to those after 30 steps time with $\Delta t = 5$. Also, with $\Delta y = 0.02$ at $\Delta t = 0.05$ or $\Delta t = 0.025$ converges at the same results. The Maple code runs faster which enable steady state results at closed trivial computational times.

4. Entropy generation analysis

The inherently irreversible of hydromagnetic flow in a saturated filled porous medium creates consistence entropy generation. Thus, this is due to exchange of energy between the fixed channel walls and conducting Eyring–Powell fluid. The local entropy volumetric generation rate for the viscous fluid for a

stimulated electric and magnetic fields is defined as (Hassan et al., 2017; Salawu and Fatunmbi, 2017):

$$I_G = \frac{k}{T_0^2}\left(\frac{dT}{d\bar{y}}\right)^2 + \frac{\mu}{T_0}\left[\left(1+\frac{1}{\rho\beta\Lambda}\right)\left(\frac{d\bar{u}}{d\bar{y}}\right)^2 - \frac{1}{6\rho\beta\Lambda^3}\left(\frac{d\bar{u}}{d\bar{y}}\right)^4\right] + \frac{\mu u^2}{T_0 K} + \frac{bu^2}{T_0\sqrt{K}} + \frac{\sigma(T)(B_0\bar{u}+E_f)^2}{T_0}. \quad (17)$$

The first term of Eq. (17) defined the irreversibility of heat transfer while the irreversibility due to magnetic field, medium porosity and fluid friction is respectively presented in the second to fifth terms of the equation. Applying equation (9), the dimensionless rate of entropy generation in Eq. (17) takes the form

$$N_s = \frac{h^2E^2I_G}{k_0T_0^2R^2} = \left(\frac{d\theta}{dy}\right)^2 + \frac{Br}{\epsilon}\left[(1+\alpha)\left(\frac{du}{dy}\right)^2 - \frac{\alpha\delta}{3}\left(\frac{du}{dy}\right)^4 + Du^2 + Fu^3 + Ha(\phi+u)^2\theta^n\right], \quad (18)$$

Taken $N_1 = \left(\frac{d\theta}{dy}\right)^2$ and $N_2 = \frac{Br}{\epsilon}\left[(1+\alpha)\left(\frac{du}{dy}\right)^2 - \frac{\alpha\delta}{3}\left(\frac{du}{dy}\right)^4 + Du^2 + Fu^3 + Ha(\phi+u)^2\theta^n\right]$

The Bejan number (Be) is described as

$$Be = \frac{N_1}{N_s} = \frac{1}{1+\varphi}, \quad (19)$$

where $\varphi = \frac{N_2}{N_1}$, $N_s = N_2 + N_1$ and N_1 illustrates the energy transfer irreversibility, N_2 depicts the magnetic field, medium porosity and fluid friction irreversibility and φ denotes the irreversibility ratio.

The Bejan number (Be) ranges from $0 \le Be \le 1$. Irreversibility as a result of magnetic field, medium porosity and fluid friction effects dominates the system when $Be = 0$, but irreversibility due to heat transfer dominate the Eyring–Powell reactive flow system when $Be = 1$ at temperature differences.

5. Results and discussion

The results of the impact of some chosen parameter values of existing studies are presented graphically. The employed parameter values are $G = 0.5$, $Ha = 0.2$, $Pr = 3$, $Br = 0.2$, $\lambda = 0.5$, $\phi = 0.3$, $m = 0.5$, $\epsilon = 0.1$, $\alpha = 0.3$, $\delta = 0.2$, $n = 1$, $D = 0.3$, $F = 0.5$ and $R = 0.01$. These are chosen as the default thermophysical parameter values except otherwise indicated on the succeeding plots.

5.1. Transient flow profiles

Figs. 2 and 3 show the effects of change in time on the flow velocity and heat distributions across the saturated porous medium. From its rest state, defined on even finer mesh, the flow momentum increases steadily until it attains the highest peak state at the centreline of the fixed horizontal channel as depicted in Fig. 2. Likewise, the fluid temperature is propelled as the time of evolution rises. The enhancement in the heat within the system as demonstrated in Fig. 3 is due to an increase in the heat source terms and thermal boundary layers. The time of achieving steady flow rate and heat state depends on the considered parameter.

Table 1
Thermal runaway computational results for different parameters.

Ha	ϕ	Br	R	ϵ	D	F	λ_c
0.5	0.3	0.2	0.01	0.1	0.3	0.5	0.961465677183
1.0	0.3	0.2	0.01	0.1	0.3	0.5	0.958000432400
0.2	0.1	0.2	0.01	0.1	0.3	0.5	0.965216394299
0.2	0.5	0.2	0.01	0.1	0.3	0.5	0.961066803030
0.2	0.3	0.4	0.01	0.1	0.3	0.5	0.962056243284
0.2	0.3	1.0	0.01	0.1	0.3	0.5	0.966089174467
0.2	0.3	0.2	0.07	0.1	0.3	0.5	0.675653843491
0.2	0.3	0.2	0.10	0.1	0.3	0.5	0.572661648183
0.2	0.3	0.2	0.01	0.3	0.3	0.5	1.062990905190
0.2	0.3	0.2	0.01	0.7	0.3	0.5	1.267422898622

5.2. Solutions dependence on parameter

The reaction of the fluid velocity and heat profiles to variational increase in the electric field loading ϕ is presented in Figs. 4 and 5. The fluid velocity reduces as the parameter values ϕ rises due to the enhancement in the magnetic field strength that induced Lorentz force which resulted in the slowdown of the fluid flow rate. Also, increasing the term ϕ encourages heat distribution in the reactive Eyring–Powell fluid flow. The parameter ϕ boosted the heat generation term within the system and thereby raises the temperature distribution.

The velocity fields for different values of the second order porosity F and Eyring–Powell material α terms is presented in Figs. 6 and 7. Both parameter oppose the reactive non-Newtonian fluid flow by increasing the fluid viscous effect at different rates, the effect in-turn diminishes the heat source term strength. The flow rate profile reduce but the effect of parameters α is well pronounced due to the viscoelastic nature of the material. Figs. 8 and 9 denote the impact of increasing the values of Brinkman number Br and Frank-Kamenetskii λ on the temperature profiles. The parameters encourages heat source term and the thermal boundary layer thickness that resulted in increasing the heat distribution rate within the saturated porous channel. Hence, enhancing the parameter values Br and λ boosted the heat field.

5.3. Solution thermal runaway

Fig. 10 is the slice bifurcation at $0 < \epsilon \ll 1$. The solution finite heat blowup is experienced due to high values of λ that resulted in large qualitative internal heat production than heat dissipation in the reactive Powell–Eyring fluid system. Thermal runaway relates to sturdily exothermic reactions that are augmented by rise in temperature. For $0 \le \epsilon \ll 1$ there exists a turning point (critical value λ_c) such that, for $0 < \lambda < \lambda_c$, the lower and upper solution branches is obtained due to the heat dependent electrical conductivity and Bimolecular kinetics in the temperature governing equation. If $\lambda_c < \lambda$, no real system solutions occurs but a classical form denoting thermal runaway is displayed. As the internal heat rises, there is decrease in the fluid viscosity. The momentum gradient increases with temperature along with rising Bimolecular kinetics and flow back into the energy equation, resulting to thermal criticality. Thermal runaway is dangerous because it can lead to explosion. Table 1 presents the computational values for thermal runaway for different parameter values. It is noticed from the table that the parameters Ha, ϕ, R reduces internal heat generation as the value increase while the parameter Br and ϵ enhance the chemical reactions internal heat production. Increasing internal heat leads to possible explosion and blowup as a result of thermal criticality state of the solution.

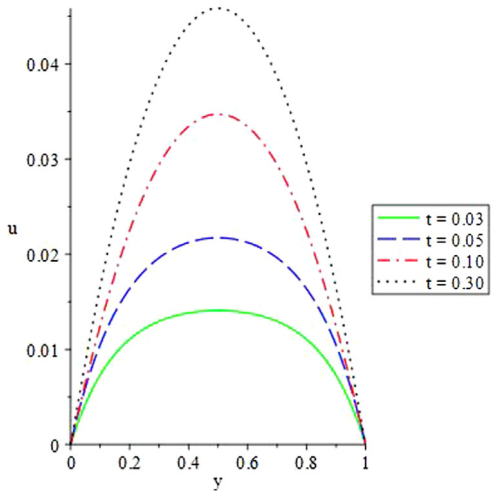

Fig. 2. Velocity profile with rising time.

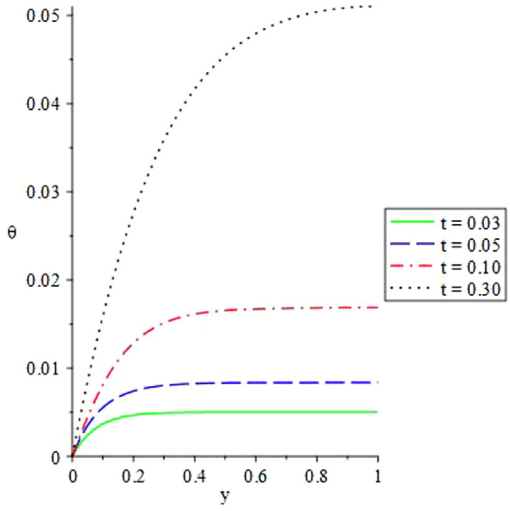

Fig. 3. Heat profile with rising time.

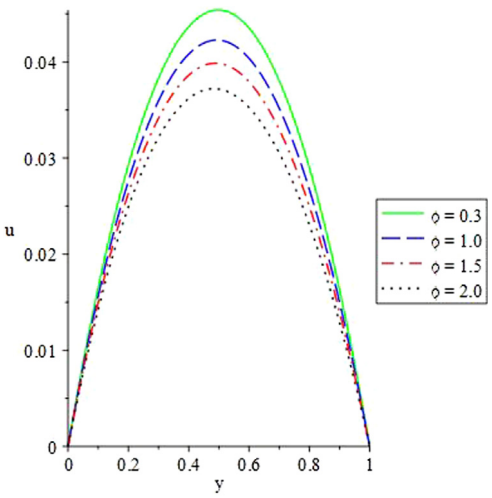

Fig. 4. Velocity profile with rising ϕ.

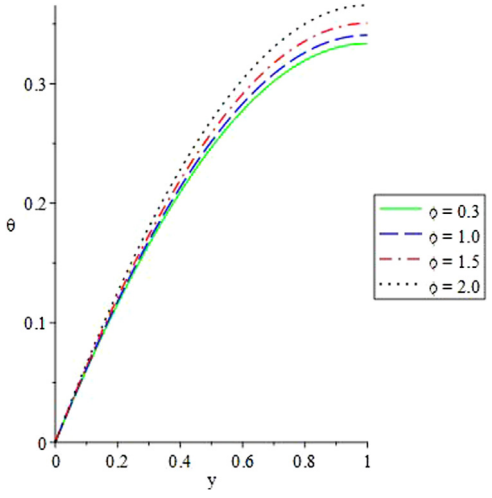

Fig. 5. Heat profile with rising ϕ.

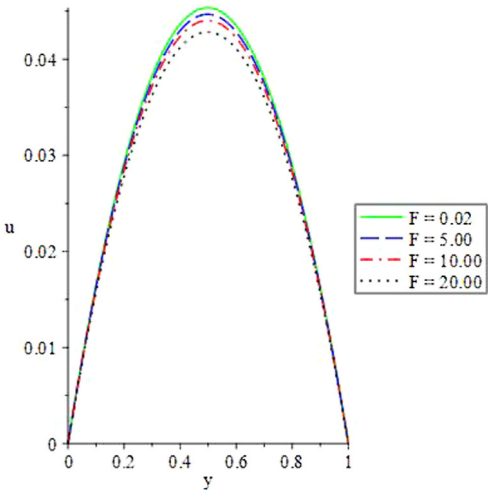

Fig. 6. Velocity profile with rising F.

5.4. Solution entropy generation and bejan number

In Figs. 11 and 12, the effects of Frank-Kamenetskii term λ on the entropy generation as result of irreversibility and Bejan number are presented. Rate of entropy generation is high at one surface of the channel and reduces gradually towards the other channel surfaces where temperature gradient occurs. The increase in the profiles is because λ is a strong heat source term that qualitatively enhances internal heat and diminishes fluid viscosity. Hence, the Bejan number and irreversibility process is significantly encouraged. Also, the impacts of thin thermal radiation R on the entropy production and Bejan number are illustrated in the plots 13 and 14. Observing from the results, the irreversibility process due to heat transfer, magnetic field, porosity, and friction dominated the reactive non-Newtonian fluid flow system to encourage entropy generation rate as seen in Fig. 13. In Fig. 14, irreversibility due to friction, porosity and magnetic field controlled lower channel surface while irreversibility as a result of heat transfer overwhelms the upper channel surface due to temperature difference that boosted the Bejan number within the saturated porous channel.

Figs. 15 and 16 depict the effects of rising in the activation energy ϵ on the entropy production rate and Bejan number. The parameter ϵ slightly increases the irreversibility process in an exothermic Bimolecular kinetic as showed in the diagram. The is expected because activation energy is a required energy for a

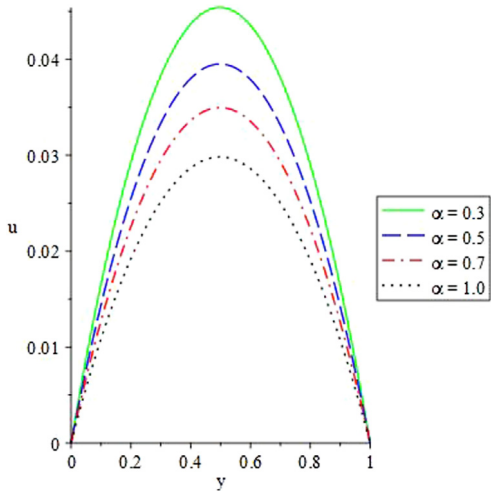

Fig. 7. Velocity profile with rising α.

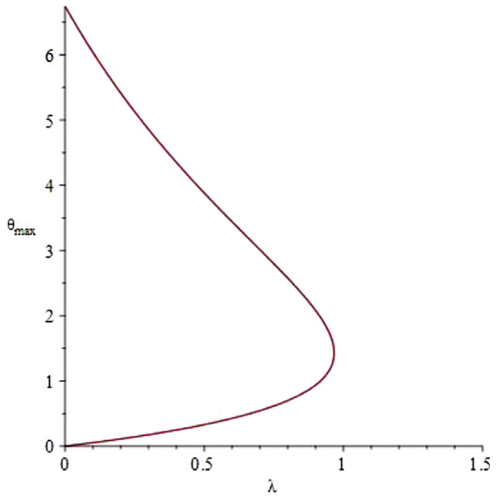

Fig. 10. Slice Approximate bifurcation.

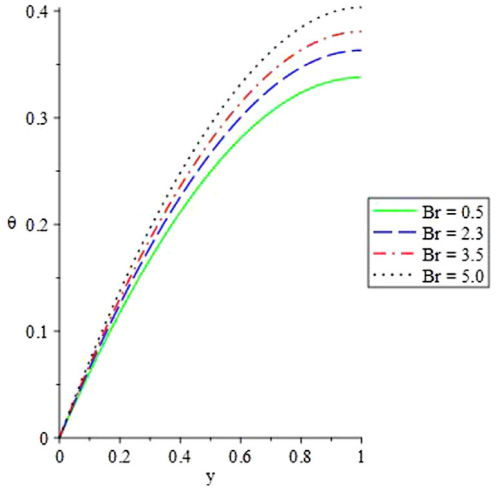

Fig. 8. Heat profile with rising *Br*.

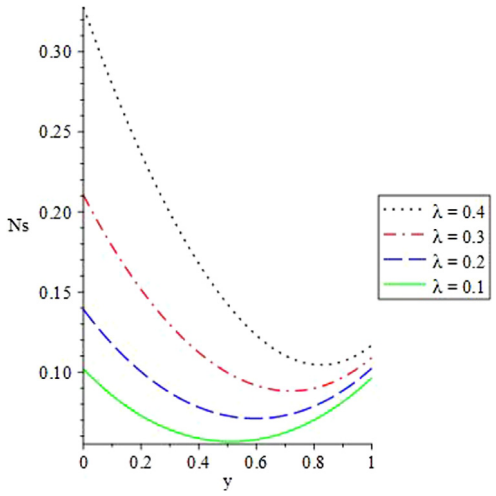

Fig. 11. Entropy generation with rising λ.

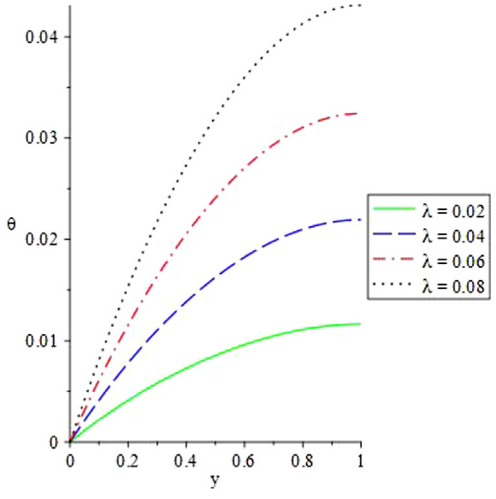

Fig. 9. Heat profile with rising λ.

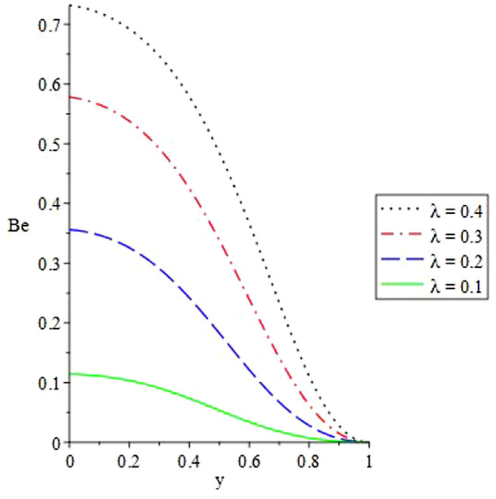

Fig. 12. Bejan number with rising λ.

reaction process to happen and for a reaction to occur an internal heat is generated moderately to start the reaction process. Then, the entropy generation and Bejan number distribution is enhanced. Figs. 17 and 18 show the reaction of irreversibility process to changes in the electric field loading parameter ϕ. The rate of entropy production and Bejan number in the reactive

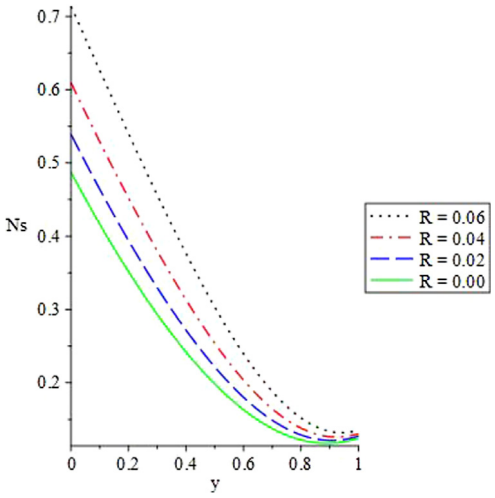

Fig. 13. Entropy generation with rising R.

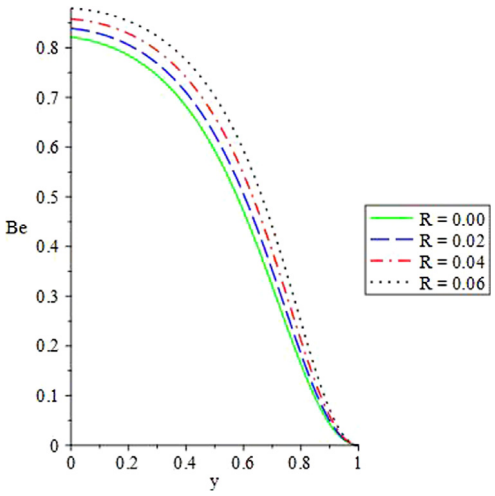

Fig. 14. Bejan number with rising R.

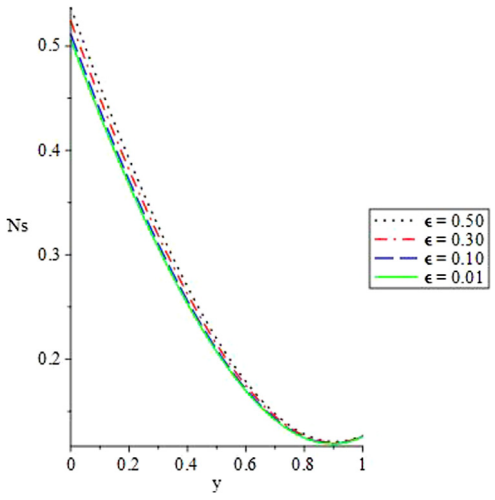

Fig. 15. Entropy generation with rising ϵ.

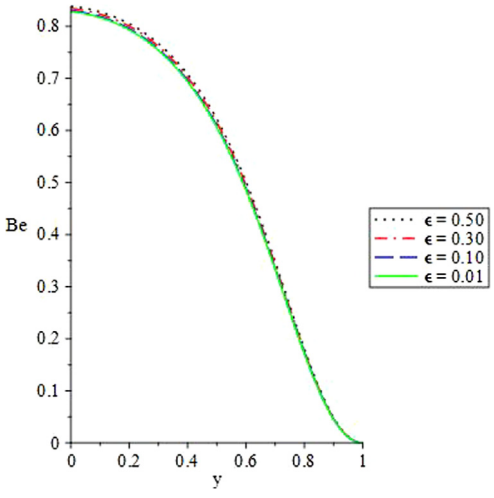

Fig. 16. Bejan number with rising ϵ.

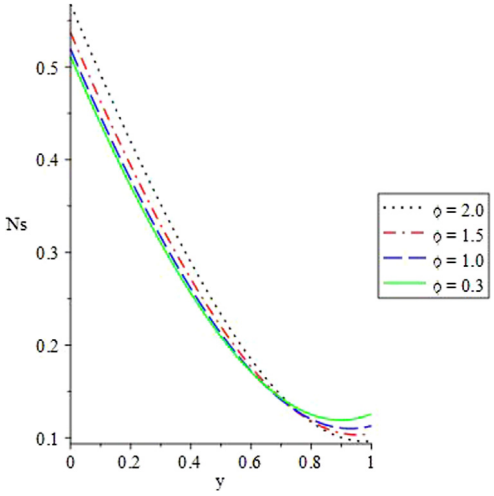

Fig. 17. Entropy generation with rising ϕ.

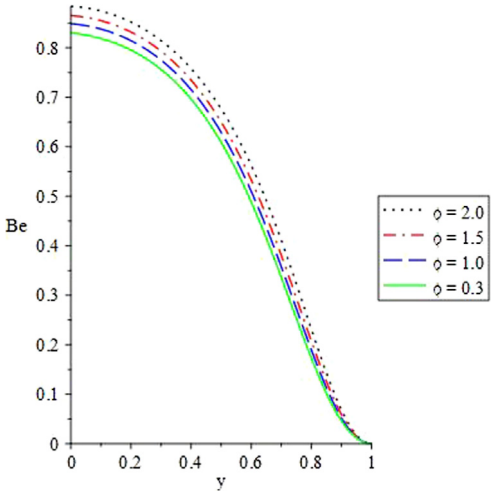

Fig. 18. Bejan number with rising ϕ.

fluid is rising slowly as portrayed in the figures. Hence, lower values of electric field loading minimized entropy generation and Bejan number in an Eyring–Powell fluid with variable electrical conductivity.

Table 2
Computational values for entropy generation and Bejan under Bimolecular kinetics.

y	N_1	N_2	$N_s = N_1 + N_2$	$\varphi = \frac{N_2}{N_1}$	$Be = \frac{1}{1+\varphi}$
0.0	0.4222830218	0.0581467914	0.4912633132	0.1376962568	0.8595859092
0.1	0.3579931027	0.0623410496	0.4263442523	0.1741403651	0.8396808465
0.2	0.2939227953	0.0696599986	0.3635827939	0.2370010075	0.8084067786
0.3	0.2334418517	0.0735103382	0.3069521899	0.3148978543	0.7605153485
0.4	0.1774959435	0.0777190172	0.2552149607	0.4378636248	0.6954762484
0.5	0.1264146237	0.0821160076	0.2085306313	0.6495768068	0.6062160888
0.6	0.0833860163	0.0874834306	0.1708694469	1.0491379072	0.4880101022
0.7	0.0475752395	0.0925184148	0.1400936543	1.9446757551	0.3395959637
0.8	0.0214092792	0.0965887816	0.1179980608	4.5115382315	0.1814375519
0.9	0.0052171872	0.1018419918	0.1070591790	19.520478746	0.0487318069
1.0	0.0000000132	0.1072182964	0.1072182832	0.0000008121	0.0000000000

Table 2 shows the computational dynamic of the entropy generation and Bejan number under Bimolecular kinetics. It is obtained from the table that as the numerical values of the entropy generation is decreasing the Bejan number value is also reducing along the saturated porous channel. If the values of the entropy production and Bejan number rise, it will increase correspondingly as reported in the graphs for a reactive Powell–Eyring fluid.

Conclusion

The study of thermal runaway and inherent irreversibility of a reactive hydromagnetic Powell–Eyring fluid flow in saturated porous media with electric field induction is examined. It is seen from the study that parameter that enhances heat source terms, encourages flow velocity and temperature while parameters that enhances fluid viscosity discourages flow velocity and heat distribution. Also, irreversibility process that leads to entropy generation in a reactive Powell–Eyring fluid can be minimized at low values of electric field loading, thin radiation, viscosity, and dissipation rate. Hence, in the study, parameters that enhances the rate of entropy production also increases the Bejan number. Moreover, the solution branches and thermal criticality conditions that demonstrated the thermal runaway of the reactive fluid is presented. It is observed that to avoid finite time blowup of the reactive Powell–Eyring solution, the choice of parameter values must be guided. Then, the parameter λ that gives estimates on the critical regimes needs conscious monitoring to avoid solution blowup. It is seen that the fluid viscosity spatial dependence is highly affected by the emerging terms of the Powell–Eyring flow explosion. Hence, this justifies the important of considering viscosity spatial dependence in exothermic reactive fluid. If the non-Newtonian term $\Lambda = 0$, the Newtonian form of the present study is obtained. The results from the study with seemly detailed chemistry approximations may be useful for various oxygen or air mixtures, hydrocarbons, fuels and many more.

Acknowledgments

The authors appreciate the management of Landmark University for their financial support and enabling environment in making the research work a reality. Also, we thank the reviewers for their comments and suggestions for the improvement of this paper.

References

Adesanya, S.O., Oluwadare, E.O., Falade, J.A., Makinde, O.D., 2015. Hydromagnetic natural convection flow between vertical parallel plates with time-periodic boundary conditions. J. Magn. Magn. Mater. 396, 295–303.

Ahmed, M.W., Khan, M.I., Hayat, T., Alsaedi, A., 2018. Entropy generation minimization (egm) of nanofluid flow by a thin moving needle with nonlinear thermal radiation. Physica B 534, 113–119.

Akbar, N.S., Abdelhalim, E., Khan, Z.H., 2015. Numerical analysis of magnetic field on eyring-powell fluid flow towards a stretching sheet. J. Magn. Magn. Mater 382, 355–358.

Baag, S., Mishra, S.R., Dash, G.C., Acharya, M.R., 2017. Entropy generation analysis for viscoelastic mhd flow over a stretching sheet embedded in a porous medium. Ain Shams Eng. J. 8, 623–632.

Bhatti, M.M., Rashidi, M.M., 2017. Numerical simulation of entropy generation on mhd nanofluid towards a stagnation point flow over a stretching surface. Int. J. Appl. Comput. Math. 3, 2275–2289.

Celli, M., Barletta, A., Longo, S., Chiapponi, L., Ciriello, V., Di Federico, V., Valiani, A., 2017. Thermal instability of a power-law fluid flowing in a horizontal porous layer with an open boundary: a two-dimensional analysis. Transp. Porous Media 0863-7.

Chinyoka, T., Makinde, O.D., 2013. Viscoelastic modeling of the diusion of polymeric pollutants injected into a pipe flow. Acta Mech. Sinica 29 (2), 166–178.

Cortell, R., 2006. A note on flow and heat transfer of a viscoelastic fluid over a stretching sheet. Int. J. Non-Linear Mech. 41, 78–85.

Di Federicoa, V., Longo, S., Chiapponi, L., Archetti, R., Ciriello, V., 2014. Radial gravity currents in vertically graded porous media: theory and experiments for newtonian and power-law fluids. Adv. Water Resour. 14, 1–32.

Gireesha, B.J., Mahanthesh, B., Rashidi, M.M., 2015. Mhd boundary layer heat and mass transfer of a chemically reacting casson fluid over a permeable stretching surface with non-uniform heat source/sink. Int. J. Ind. Math. 7 (14).

Govindaraju, M., Saranya, S., Hakeem, A.K.A., Jayaprakash, R., Ganga, B., 2015. Analysis of slip mhd nanofluid flow on entropy generation in a stretching sheet. Proc. Eng. 127, 501–507.

Hassan, A.R., Maritz, R., Gbadeyan, J.A., 2017. A reactive hydromagnetic heat generating fluid flow with thermal radiation within porous channel with symmetrical convective cooling. Int. J. Therm. Sci. 122, 248–256.

Hayat, T., Ali, S., Alsaedi, A., Alsulami, H.H., 2016. Influence of thermal radiation and joule heating in the eyring-powell fluid flow with the soret and dufour effects. J. Appl. Mech. Tech. Phys. 57, 1051–1060.

Hayat, T., Awais, M., Asghar, S., 2013. Radiative effects in a three dimensional flow of MHD eyring-powell fluid. J. Egypt Math. Soc. 21, 379–384.

Hayat, T., Khan, M.I., Qayyum, S., Alsaedi, A., 2018. Entropy generation in flow with silver and copper nanoparticles. Colloids Surf. A 539, 335–346.

Hayat, T., Nawaz, S., Alsaedi, A., 2017. Entropy generation in peristalsis with different shapes of nanomaterial. J. Mol. Liq. 248, 447–458.

Ireka, I.E., Chinyoka, T., 2013. Non-isothermal flow of a johnsonsegalman liquid in a lubricated pipe with wall slip. J. Non-Newton. Fluid Mech. 192, 20–28.

Jalil, M., Asghar, S., Imran, S.M., 2013. Self similar solutions for the flow and heat transfer of powell-eyring fluid over a moving surface in a parallel free stream. Int. J. Heat Mass Transfer 65, 73–82.

Khan, M.I., Hayat, T., Khan, M.I., Alsaedi, A., 2018. Activation energy impact in nonlinear radiative stagnation point flow of cross nanofluid. Int. Commun. Heat Mass Trans. 91, 216–224.

Longo, S., Di Federico, V., Archetti, R., Chiapponi, L., Ciriello, V., Ungarish, M., 2013b. On the axisymmetric spreading of non-newtonian power-law gravity currents of time-dependent volume: an experimental and theoretical investigation focused on the inference of rheological parameters. J. Non-Newton. Fluid Mech. 13, 1–46.

Longo, S., Di Federico, V., Chiapponi, L., 2015. A dipole solution for power-law gravity currents in porous formations. J. Fluid Mech. 778, 534–551.

Longo, S., Di Federico, V., Chiapponi, L., Archetti, A., 2013a. Experimental verification of power-law non-newtonian axisymmetric porous gravity currents. J. Fluid Mech. 731, 1–12.

Mahanthesh, B., Gireesha, J., Reddy Gorla, R.S., 2017. Eyring-powell fluid past a convectively heated stretching sheet in the presence of thermal radiation, viscous dissipation and joule heating. J. Assoc. Arab Univ. Basic Appl. Sci. 23, 75–82.

Makinde, O.D., Chinyoka, T., 2010. Numerical investigation of transient heat transfer to hydromagnetic channel flow with radiative heat and convective cooling. Commun. Nonlinear Sci. Numer. Simul. 15, 3919–3930.

Ogunseye, A., Okoya, S.S., 2017. Criticality and thermal explosion in the flow of reactive viscous third grade fluid flow in a cylindrical pipe with surface cooling. J. Nigerian Math. Soc. 36 (2), 399–418.

Okoya, S.S., 2011. Disappearance of criticality for reactive third-grade fluid with reynold's model viscosity in a flat channel. Int. J. Non-Linear Mech. 46, 1110–1115.

Rehman, K.U., Malik, M.Y., Bilal, S., Bibi, M., Ali, U., 2017. Logarithmic and parabolic curve fitting analysis of dual stratified stagnation point mhd mixed convection flow of eyring-powell fluid induced by an inclined cylindrical stretching surface. Results Phys. 7, 544–552.

Rehman, K.U., Malik, M.Y., Salahuddin, T., Naseer, M., 2016. Dual stratified mixed convection flow of eyring-powell fluid over an inclined stretching cylinder with heat generation/absorption effect. AIP Adv. 6, 075112.

Rundora, L., Makinde, O.D., 2018. Unsteady mhd flow of non-newtonian fluid in a channel filled with a saturated porous medium with asymmetric navier slip and convective heating. Appl. Math. Inf. Sci. 12 (3), 483–493.

Salawu, S.O., Dada, M.S., 2016. Radiative heat transfer of variable viscosity and thermal conductivity effects on inclined magnetic feld with dissipation in a non-darcy medium. J. Nigerian Math. Soc. 35, 93–106.

Salawu, S.O., Fatunmbi, E.O., 2017. Inherent irreversibility of hydromagnetic third-grade reactive poiseuille flow of a variable viscosity in porous media with convective cooling. J. Serb. Soc. Comput. Mech. 11 (1), 46–58.

Salawu, S.O., Ogunseye, H.A., Olanrewaju, A.M., 2018. Dynamical analysis of unsteady poiseuille flow of two-step exothermic non-newtonian chemical reactive fluid with variable viscosity. Int. J. Mech. Eng. Technol. 9 (12), 596–605.

Salawu, S.O., Okedoye, A.M., 2018. Thermodynamic second law analysis of hydromagnetic gravity-driven two-step exothermic chemical reactive flow with heat absorption along a channel. Iran. J. Energy Environ. 9 (2), 114–120.